

Shape-Based Hand Recognition

Erdem Yörük, Ender Konukoğlu, Bülent Sankur, *Senior Member, IEEE*, and Jérôme Darbon

Abstract—The problem of person recognition and verification based on their hand images has been addressed. The system is based on the images of the right hands of the subjects, captured by a flatbed scanner in an unconstrained pose at 45 dpi. In a pre-processing stage of the algorithm, the silhouettes of hand images are registered to a fixed pose, which involves both rotation and translation of the hand and, separately, of the individual fingers. Two feature sets have been comparatively assessed, Hausdorff distance of the hand contours and independent component features of the hand silhouette images. Both the classification and the verification performances are found to be very satisfactory as it was shown that, at least for groups of about five hundred subjects, hand-based recognition is a viable secure access control scheme.

Index Terms—Independent component analysis, modified Hausdorff distance, pose registration.

I. INTRODUCTION

THE emerging field of biometric technology addresses the automated identification of individuals, based on their physiological and behavioral traits. The broad category of human authentication schemes, denoted as biometrics encompasses many techniques from computer vision and pattern recognition. The personal attributes used in a biometric identification system can be physiological, such as facial features, fingerprints, iris, retinal scans, hand and finger geometry; or behavioral, traits idiosyncratic of an individual, such as voice print, gait, signature, and keystroke style. Depending on the complexity or the security level of the application, one will opt to use one or more of these personal characteristics, possibly under a multimodal fusion scheme for performance enhancing [14].

In this paper, we investigate the shape of the hand silhouette as a distinctive personal attribute for an authentication task. Despite the fact that the use of hands as biometric evidence is not very new, and that there are an increasing number of commercial products actually deployed, the documentation in the literature is scarce as compared to other modalities like face or voice. One distinct advantage the hand modality offers is that its imaging conditions are less complex, for example a relatively

simple digital camera or flatbed scanner would suffice. Consequently, hand-based biometry is user-friendlier and it is less prone to disturbances and more robust to environmental conditions and to individual anomalies. In contrast, face modality is known to be quite sensitive to pose, facial accessories, expression, and lighting variations; iris or retina-based identification requires special illumination and is much less friendly; fingerprint imaging requires good frictional skin, etc., and up to 4% of the population may fail to get enrolled [14]. Therefore, authentication based on hand shape can be an attractive alternative due to its unobtrusiveness, low-cost, easy interface, and low data storage requirements. Some of the presently deployed access control schemes based on hand geometry range from passport control in airports to international banks, from parents' access to child daycare centers to university student meal programs, from hospitals, prisons, to nuclear power plants [27]. In fact, there exist a number of patents on hand information-based personnel identification, using either geometrical features or on hand profile [27].

Most of the hand-based biometric schemes in the literature fall into the broad category of geometric features of the hand. For example, Sanchez-Reillo *et al.* [22] select 25 features, such as finger widths at different latitudes, finger and palm heights, finger deviations and the angles of the interfinger valleys with the horizontal, and model them with Gaussian mixtures. Jain *et al.* [21] have used a peg-based imaging scheme and obtained 16 features, which include length and width of the fingers, aspect ratio of the palm to fingers, and thickness of the hand. The prototype system they developed was tested in a verification experiment for web access over for a group of ten people [20]. Kumar *et al.* [2], [28] extract geometric features similar to [19], [21], and [22]. Öden *et al.* [19], in addition to geometric features such as finger widths at various positions and palm size, have made use of finger shapes. These shapes have been represented with fourth degree implicit polynomials, and the resulting sixteen features are compared with the Mahalanobis distance. A recent work utilizes both hand geometry and palm print information as in Kumar *et al.* [17], which use decision level fusion. Finally, there are schemes that employ solely palmprint information, such as in Han *et al.* [11] and Zhang [26].

In our paper, we employ a global hand shape-based approach for person identification and verification. The algorithm is pivoted on the normalization of the deformable hand shape. In other words, "hand shape normalization" involves the registration of fingers by separate rotations to standard orientations as well as the rotation and translation of the whole hand. Subsequently, person identification is based on the comparison of the hand silhouette shapes using Hausdorff distance or on the distance of feature vectors, namely the independent component analysis (ICA) features. The first part of the method of Jain and Duta [8] is

Manuscript received September 18, 2004; revised July 12, 2005. This work was supported in part by the Bogazici University Research Fund 03A201 and in part by the TUBITAK Research Project 102E027. The associate editor coordinating the review of this manuscript and approving it for publication was Dr. Hassan Foroosh.

E. Yörük and E. Konukoğlu are with the BUSIM Laboratory, Boğaziçi University, 34342 Istanbul, Turkey (e-mail: yoruk.erdem@gmail.com; ender.konukoglu@gmail.com).

B. Sankur is with Boğaziçi University, 34342 Istanbul, Turkey (e-mail: bulent.sankur@boun.edu.tr).

J. Darbon is with the EPITA Research and Development Laboratory and Ecole Nationale Supérieure des Télécommunications, Paris, France (e-mail: jerome.darbon@lrde.epita.fr).

Digital Object Identifier 10.1109/TIP.2006.873439

TABLE I
CHARACTERISTICS AND POPULATION SIZES OF THE HAND-BASED RECOGNITION ALGORITHMS

Algorithm	Features & Classification	Number of subjects	Total number of images tested/Image per subject
Oden et al. [19]	16 features: geometric features and implicit polynomial invariants of fingers. Classifier based on Mahalanobis distance.	27	270/10
Sanchez-Reillo et al. [22]	25 geometric features including finger and palm thickness. Classifier based on Gaussian mixture models.	20	200/10
Duta-Jain [8]	Hand contour data. Classifier based on mean average distance of contours.	53	353/variable
Ross [21]	16 geometric features including length, height and thickness of fingers and palm. Classifier based on Euclidean and Mahalanobis distances.	50	360/variable
Bulatov et al. [2]	30 geometric features including length and height of fingers and palm. Classifier based on Chebyshev metric between feature vectors.	70	714/10
Kumar [17]	160 combined features, 16 coming hand geometry and remaining 144 from palmprint images. Classifier based on correlation-like similarity measure.	100	1000/10
Our methods	1 st method: Features consist of hand contour data. Classifier based on modified Hausdorff distance. 2 nd method: Features consist of independent components of the hand silhouette. Classifier based on the Euclidean distance.	458	1374/3

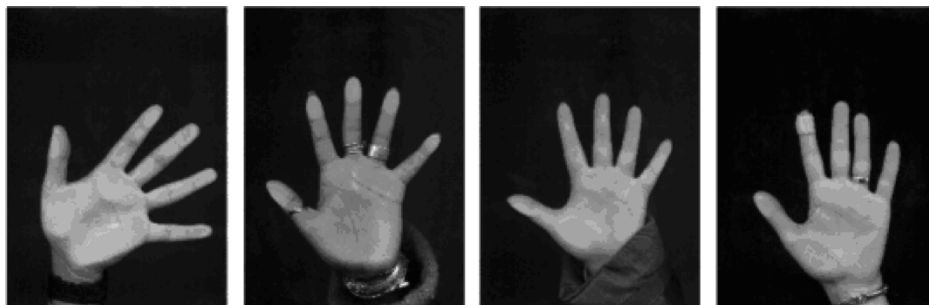


Fig. 1. Sample hand images with unconstrained pose and accessories.

somewhat similar to ours in that they compare the contour shape difference via the mean square error, and it involves finger alignment. The features used and the data sizes in different algorithms are summarized in Table I.

We assume that the user of this system will be cooperative, as he/she would be demanding for access. In other words, the

user would have no interest in invalidating the access mechanism by moving or jittering his/her hand or by having fingers crumpled or sticking to each other. On the other hand, the implementation does not assume or force the user to any particular orientation. A variety of hand postures are illustrated in Fig. 1, where the only assumption is that the fingers are not touching

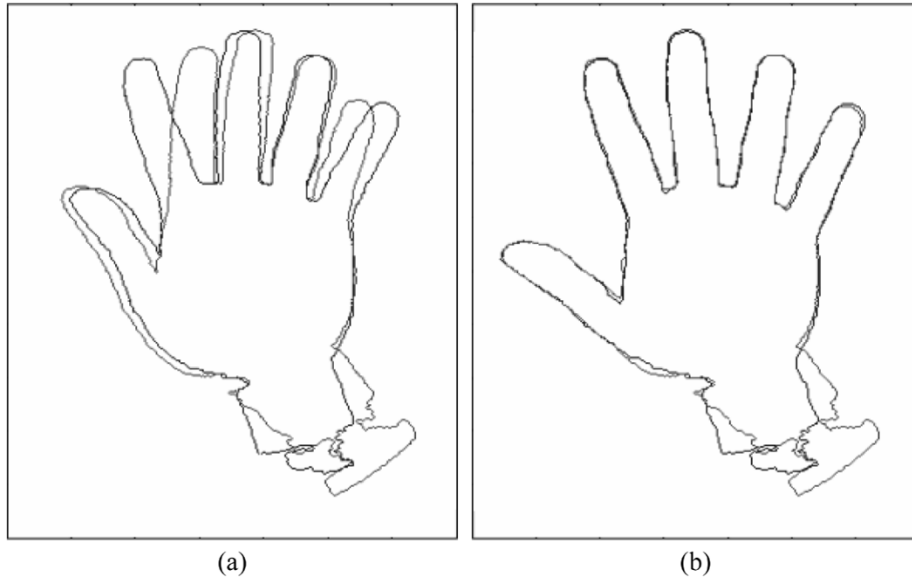


Fig. 2. Two superposed contours of the hand of the same individual: (a) rigid hand registration only and (b) finger alignment after hand registration.

or curved around knuckles. The orientation information of the hand/fingers is automatically recovered from the scanned image and then the hand is normalized.

The paper is organized as follows. In Section II, the segmentation of hand images and their normalization to compensate for their deformable shape are given. Section III discusses the computation of features from the normalized hand silhouettes. The experimental setup and the classification results are discussed in Section IV, and conclusions are drawn in Section V.

II. NORMALIZATION OF HAND CONTOURS

A. Hand Segmentation

The hand segmentation aims to extract the hand region from the background. At first sight, segmentation of a two-object scene, consisting of a hand and the background, seems a relatively easy task. However, segmentation accuracy may suffer from artifacts due to rings, overlapping cuffs or wristwatch belts/chains, or creases around the borders from too light or heavy pressing. Furthermore, the delineation of the hand contour must be very accurate, since the differences between hands of different individuals are often minute. We have comparatively evaluated two alternate methods of segmentation, namely, clustering followed by morphological operations and the watershed transform-based segmentation. Since both methods work competitively well, we preferred the less complex clustering approach. Interestingly enough, the Canny edge-based segmentation with snake completion [4], [25] did not work well due to the difficulty of fitting snakes to the very sharp concavities between fingers. Snake algorithms performed adequately only if they were properly initialized at the extremities.

We have used the K-means clustering algorithm on both the gray-level pixels and the RGB color components to separate the hand foreground and the darker background. Both gave identical results, hence the simpler gray-level clustering was preferred. However, without any postprocessing the resulting maps may end up having holes and isolated foreground blobs,

as well as severed fingers due to accessories. We therefore find the largest connected components in the foreground, and then remove the debris by using area-based size filtering. However, lest a smaller connected components be a severed finger due to ring artifacts, we check for the second up to sixth ranking components. The “ring artifact removal” algorithm (explained in Section II-C) then corrects any straights or isthmuses caused by the presence of rings. Similarly, we accept as background the largest connected component obtained from the reverse image. This background image is similarly processed with area-based filtering.

The normalization of hand images involves the registering of hand images, that is global rotation and translation, as well as re-orienting fingers individually along standardized directions, without causing any shape distortions. This is, in fact, the most critical operation for a hand-shape based biometry application whenever global features are used. There are however schemes that use only local features [2], [19], for example separate contours of fingers, for which such a normalization is not warranted. The necessity of finger re-orientation is illustrated in Fig. 2, and it was also pointed out in [8]. This figure shows hand images of the same person taken on two different sessions. The left figure is the contour after global hand registration (but not yet finger registration), while the figure on the right is the outcome after registration of fingers. The registration process involves two steps: 1) translation to the centroid of the hand such that it coincides with the center of the image; 2) rotation toward the direction of the larger eigenvector, that is the eigenvector corresponding to the larger eigenvalue of the inertia matrix. The inertia matrix is simply the 2×2 matrix of the second-order centered moments of the binary hand pixel distances from their centroid. A brief reminder of the inertial matrix is as follows. Consider the moments of a binary image

$$m_{i,j} = \sum_{(x,y) \in \text{object}} x^i y^j \quad (1)$$

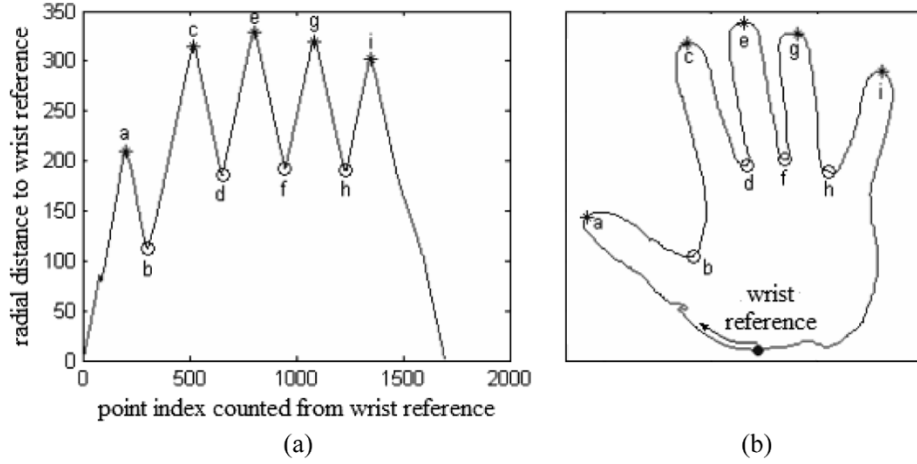


Fig. 3. (a) Radial distance function for finger extraction and (b) a hand contour with marked extremities.

where the summation is over the object pixels. The centroid is defined as

$$\bar{x} = \frac{m_{1,0}}{m_{0,0}} \quad (2)$$

$$\bar{y} = \frac{m_{0,1}}{m_{0,0}}. \quad (3)$$

Therefore, the central moments can be written as

$$\mu_{i,j} = \sum_{(x,y) \in \text{object}} (x - \bar{x})^i (y - \bar{y})^j. \quad (4)$$

The inertial matrix (i.e., sample covariance matrix of the object coordinates) then becomes

$$\mathbf{I} = \begin{bmatrix} \mu_{2,0} & \mu_{1,1} \\ \mu_{1,1} & \mu_{0,2} \end{bmatrix} \quad (5)$$

and the orientation of the object is given by the direction of the major eigenvalue. It can be shown that this angle is given by [24]

$$\theta = 0.5 \arctan \left(\frac{2\mu_{1,1}}{\mu_{2,0} - \mu_{0,2}} \right). \quad (6)$$

Obviously, unless fingers have been set to standard orientations, recognition performance will remain very poor, as the relative distance or shape discrepancy between these two superimposed images (intra-difference) can easily exceed the distance between hands belonging to different individuals (interdifference). The steps of the hand normalization algorithm are given in Section II-D and E.

B. Localization of Hand Extremities

Detecting and localizing the hand extremities, that is, the fingertips and the valley between the fingers is the first step for hand normalization. Since both types of extremities are characterized by their high curvature, we first experimented with curvogram of the contour, that is, the plot of the curvature of the contour at various scales along the path length parameter. The nine maxima in the curvogram, which were consistent across all scales, were taken as the sought after hand extremities. However, we observed that this technique was rather sensitive to

contour irregularities, such as spurious cavities and kinks, especially around the ill-defined wrist region.

A more robust alternative technique was provided by the plot of the radial distance with respect to a reference point around the wrist region. This reference point was taken as the first intersection point of the major axis (the larger eigenvector of the inertial matrix) with the wrist line. The resulting sequence of radial distances yields minima and maxima corresponding to the sought extremum points. The resulting extrema are very stable since the definition of the five maxima (fingertips) and four minima are not affected by the contour irregularities. The radial distance function and a typical hand contour with extremities marked on it are given in Fig. 3.

C. Ring Artifact Removal

The presence of rings may cause severance of the finger from the palm or may create an isthmus on the finger [Fig. 4(a)]. First, an isolated finger can be detected simply by the size of its connected component since on one side, its size is far larger than any background debris removed with morphological filtering, and on the other side it is always smaller than the main body of the hand. A severed finger can be reconnected to its hand by prolonging its sides in straight lines till it meets the palm. These straight lines skim past the sides of the finger parallel to its major axis direction.

Second, the presence of an isthmus due to faulty segmentation of a ring [see Fig. 4(b)] can be detected by monitoring the contour distance to the finger's major axis. Any local minimum on the left and/or right side of a finger, that is any time the distance exceeds a threshold, it is assumed to be a cavity caused by the ring. We have set this threshold to one quarter of the distance median between the major axis and the left and right profiles of a finger. The isthmus effect is eventually repaired by bridging over the cavities with straight lines and filling in inside the bays by interpolation.

D. Finger Registration

Having located all five fingers by the extremities on the radial sequence one can start dealing with the hand normalization. The hand normalization algorithm consists of the following steps (see Fig. 5).

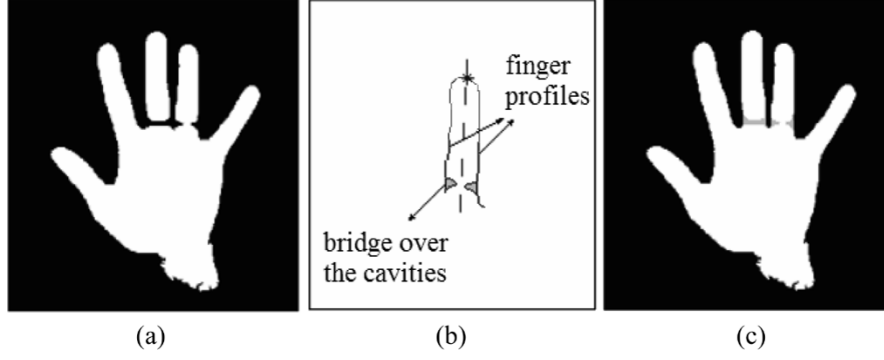


Fig. 4. (a) Severed middle finger and a ring finger with isthmus, (b) detail of finger isthmus; and (c) hand image after ring artifact removal.

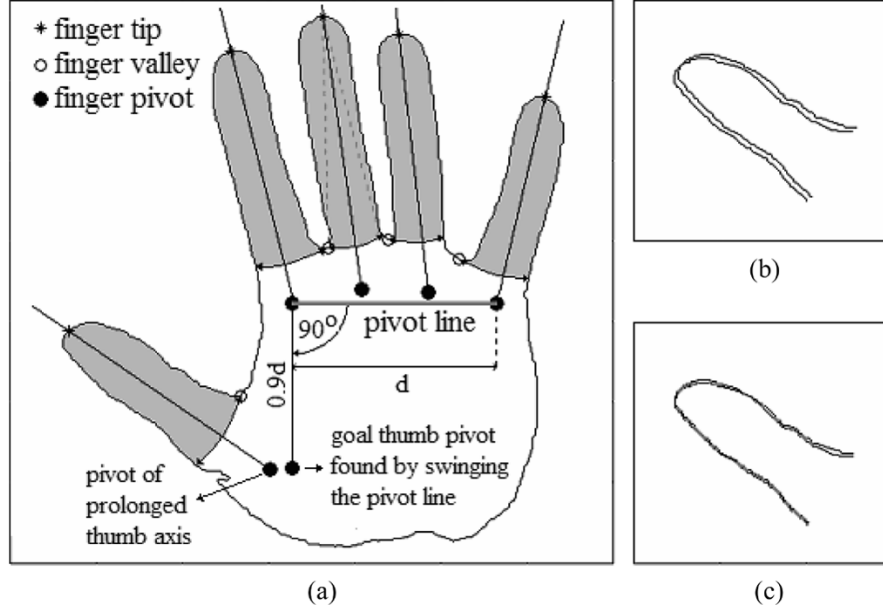


Fig. 5. (a) Fingers extracted by a sickle sweep, finger axes, finger pivots, and definition of hand pivotal axis; (b) thumbs of the same person overlapped after rotation; and (c) thumbs of the same person overlapped after rotation and pivotal translation.

1) *Extracting Fingers:* Starting from the finger extremities found in Section II-B, one draws segments from the tip along the finger side toward the two adjacent valley points. The shorter of these two segments is chosen, and then it is swung like a pendulum toward the other side. This sickle sweep delineates neatly the finger and its length can thus be computed [Fig. 5(a)]. This extraction operation, however, is somewhat different for the thumb.

2) *Finger Pivots:* Fingers rotate around the joint between proximal phalanx and the corresponding metacarpal bone. Recall that the metacarpus is the skeleton of the hand between the wrist and the five fingers. This skeleton consists of five long bones, which take place between the wrist bones and the finger bones (phalanges), as in [3]. These joints are somewhat below the line joining the interfinger valleys. Therefore, the major axis of each finger is prolonged toward the palm by 20% in excess of the corresponding finger length (determined in part a), as shown in Fig. 5(a). The ensemble of end-points of the four fingers axes (index, middle, ring, little) establishes a line, which depends on the size and orientation of the hand.

3) *Hand Pivotal Axis:* The set of four finger pivots (index, middle, ring, little) constitute a good reference for all sub-

sequent hand processing steps. A pivotal line is established that passes through these four points by least squares or by simply joining together the pivots of the index and little fingers [Fig. 5(a)]. We call this line, the pivot line of the hand. The pivot line serves several purposes: first, to register all hand images to a chosen pivot line angle (this angle was chosen as 80° with respect to the x axis). Second, the rotation angles of the finger axes are always computed with respect to the pivot line. Finally, the orientation and size of the pivot line helps us to register the thumb and to establish the wrist region.

Rotation of the fingers: We calculate the major axis of each finger from its own inertial matrix and calculate its orientation angle θ . Each finger i is rotated by the angle $\Delta\theta_i = \theta_i - \psi_i$, for i = index, middle, ring, little, and where ψ_i is the goal orientation of that finger. The finger rotations are effected by multiplying the position vector of the finger pixels by the rotation matrix

$$\mathbf{R}_{\Delta\theta} = \begin{bmatrix} \cos \Delta\theta & -\sin \Delta\theta \\ \sin \Delta\theta & \cos \Delta\theta \end{bmatrix} \quad (7)$$

around their pivot. The standard angles of the fingers are deduced from an average hand and are given in Table II. Note

TABLE II
ANGLES FOR THE FINGERS OF THE PROTO-HAND GIVEN IN DEGREES

Thumb	Index	Middle	Ring	Little
150	120	100	80	60

again that the subject is free to place his hand with arbitrary finger postures, and our algorithm will register them to the standard angles. Obviously any other angle set would work equally well in our algorithm, provided the alternative angle set leaves the fingers apart. However, the angles recommended in Table II correspond to a natural posture: extreme angles could strain and distort the hand image.

4) *Processing for the Thumb*: The motion of the thumb is somewhat more complicated since it involves rotations with respect to two separate joints. In fact, both the metacarpal-phalanx joint as well as the trapezium-metacarpal joint play a role in the thumb motion. We have compensated for this relatively more complicated displacement by a rotation followed by a translation. A concomitant difficulty is the fact that the stretched skin between the thumb and the index finger confuses the valley determination and thumb extraction. For this purpose, we rely on the basic hand anatomy, and the thumb is assumed to measure the same length as the person's little finger. A line along the major axis of the thumb is drawn and a point on this line, which measures from the tip of the thumb by 120% of the size of the little finger, forms the thumb pivot. The thumb is then translated so that its pivot coincides with the tip of the hand pivot line, when the latter is swung 90° clockwise. The thumb is finally rotated to its final orientation and merged back into the hand [Fig. 5(a)]. Two of the thumb images, before and after normalization, are shown in Fig. 5(b). Notice that the thumb can potentially arrive in a curved posture that would make the processing more complicated. However, the pressure that the subject exerts on the platen, even a light one, helps to straighten out all fingers. In any case, among the 3000 hand images an invalid thumb did not occur.

After normalizing finger orientations, the hand is translated so that its centroid, defined as the mean of the four pivot points, is moved to a fixed reference point in the image plane. Finally, the whole hand image is rotated so that its pivot line aligns with a fixed chosen orientation. Alternatively, the hands could be registered with respect to their major inertial axis and centered with respect to the centroid of the hand contours (and not the pivotal centroid).

One can envision enforcing the subject to have identical finger orientations via the use, e.g., of pegs. However, pegs not only bring in additional constraint precluding, for example, noncontact image capture, but also desired precision cannot be attained due to varying pressure of the hand on the platen or tension in the fingers. Furthermore, even with pegs one needs some re-orientation and normalization.

E. Wrist Completion

The hand contours we obtain after segmentation have irregularities in the wrist regions, which occur due to clothing or the difference in the angle of the forearm and the pressure exerted

on the imaging device. These irregularities cause different wrist segments in every hand image taken, which can adversely affect the recognition rate. The solution to this problem is to create a uniform wrist region consistent for every hand image and commensurate with its size.

We investigated two approaches to synthesize a wrist boundary. The first approach is a curve completion algorithm called the Euler spiral [16]. The Euler spiral furnishes a natural completion of a contour, when certain parts of this contour are missing, e.g., due to occlusion. The information needed for the filling of the contour gap is the two end points and their respective slopes. In the Euler spiral reconstitution of the wrist the two endpoints were taken at a distance of 1.5 times the length of the thumb and of the little finger, as measured from their respective fingertips. The endpoint slopes were computed by averaging the slope over 15 contour elements upstream from the endpoints. An example of the "Euler wrist" is shown in Fig. 6(b).

A simpler alternative would be to guillotine the hand at the same latitudes, in other words to connect the two sides of the palm by a straight line at the latitude of one pivot line length, parallel and below the pivot line. An example of guillotined wrist is shown in Fig. 6(c). Although both alternatives result in visually plausible wrists, we observed that in experiments there resides still some uncertainty adversely affecting correct recognition. We therefore decided to discount the wrist region by attaching a low weight [18] in the recognition using Hausdorff distance. Similarly, for the hand images [Fig. 6(d)], we applied a cosine taper starting from the half distance between the pivot line and the wrist line.

III. FEATURE EXTRACTION AND RECOGNITION

There are several choices for the selection of features in order to discriminate between hands in a biometric application. We used comparatively two hand recognition schemes that are quite different in nature. The first method is based on distance measure between the contours representing the hands, and hence it is shape-based. The second recognition scheme considers the whole scene image containing the normalized hand and its background, and applies subspace methods. Thus, the second method can be considered as an appearance-based method, albeit the scene is binary consisting of the silhouette of the normalized hand. However, this approach can equally be applied to gray-level hand images, which would include hand texture and palm print patterns.

A. Modified Hausdorff Distance

In order to compare different hand geometries, the Hausdorff distance is an effective method. This metric has been used in binary image and shape comparison and computer vision for a long time [7]. The advantage of Hausdorff distance over binary correlation is the fact that this distance measures proximity rather than exact superposition; thus, it is more tolerant to perturbations in the locations of points. Given the sets $F = \{f_1, f_2, \dots, f_{N_f}\}$ and $G = \{g_1, g_2, \dots, g_{N_g}\}$, where $\{f_i\}$ and

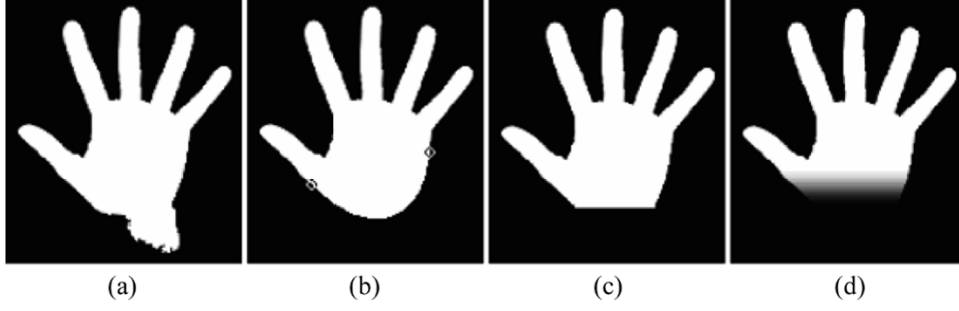


Fig. 6. (a) Hand after finger normalization and global rotation, (b) completion of the wrist based on Euler spiral, (c) wrist formed with a guillotine cut, and (d) wrist tapered after guillotine cut with square of cosine function.

$\{g_j\}$ denote contour pixels of two hands for $i = 1, \dots, N_f$ and $j = 1, \dots, N_g$, the Hausdorff distance is defined as

$$H(F, G) = \max(h(F, G), h(G, F)) \quad (8)$$

where

$$h(F, G) = \max_{f \in F} \min_{g \in G} \|f - g\|. \quad (9)$$

In this formula, $\|f - g\|$ is a norm over the elements of the two sets and obviously the contour pixels (f, g) run over the set of indexes $i = 1, \dots, N_f$ and $j = 1, \dots, N_g$. In our case, this norm is taken to be the Euclidean distance between the two points. Since the original definition of the Hausdorff distance is rather sensitive to noise, we opted to use a more robust version of this metric, namely the modified Hausdorff distance, defined as in [7] and [23]

$$h(F, G) = \frac{1}{N_f} \sum_{f \in F} \min_{g \in G} \|f - g\| \quad (10)$$

$$h(G, F) = \frac{1}{N_g} \sum_{g \in G} \min_{f \in F} \|f - g\| \quad (11)$$

where N_f and N_g are the numbers of points in sets F and G , respectively.

B. Features From Independent Component Analysis

The Independent Component Analysis (ICA) is a technique for extracting statistically independent variables from a mixture of them. It has been successfully used in many different applications for finding hidden factors within data to be analyzed or decomposing it into the original source signals. In the context of natural images, it also serves as a useful tool for feature extraction and person authentication tasks [1], [6]. In this paper, we apply the ICA tool on binary images to extract and summarize prototypical shape information. Notice that this is a novel application of this decomposition technique, in that the applications in the literature are almost always on gray-level images. In other words, while the applications [1], [6] use both shape and texture information for decomposition, we use solely binary silhouettes as the input to the source separation algorithm. The ICA algorithm, however, has been applied on one-dimensional binary source signals, which were mixed via OR operation in [12].

ICA assumes that each one of the observed signals $\{x_i(k), k = 1, \dots, K\}$ is a mixture of a set of N unknown independent source signals s_i , through an unknown mixing matrix \mathbf{A} . With \mathbf{x}_i and \mathbf{s}_i ($i = 1, \dots, N$) forming the rows of the $N \times K$ matrices \mathbf{X} and \mathbf{S} , respectively, we have the following model:

$$\mathbf{X} = \mathbf{AS}. \quad (12)$$

The data vectors for the ICA decomposition are the lexicographically ordered hand image pixels. The dimension of these vectors is K (for example, $K = 40000$, if we assume a 200×200 hand image). More specifically, the \mathbf{X} matrix consists of columns, which are formed from the lexicographically ordered segmented hand image scenes, that is, hand plus the background. In other words, each column corresponds to one whole image. Thus, the data matrix \mathbf{X} consists of N (number of subjects) columns and K rows (number of pixels in the segmented image). Despite the fact that the binary image, and as a matter of fact the gray-level image may contain any number of zero rows/columns, the whole lexicographic reading of the image is never a zero vector due to the two-class clustering in Section II-A. Therefore, there is never any risk for the covariance matrix to be singular or the basis vectors to be identical in the mixing matrix. The only vanishingly improbable case of a singular covariance matrix might occur if one K long (e.g., 40000 long) binary vector is a linear combination of some other ones.

Briefly, ICA aims to find a linear transformation \mathbf{W} for the inputs that minimizes the statistical dependence between the output components \mathbf{y}_i , the latter being estimates of the hypothesized independent sources \mathbf{s}_i

$$\hat{\mathbf{S}} = \mathbf{Y} = \mathbf{WX}. \quad (13)$$

In order to find such a transformation \mathbf{W} , which is also called separating or de-mixing matrix, we implemented the fastICA algorithm [13] that maximizes the statistical independence between the output components using maximization of their negentropy. There exists two possible formulation of ICA [1], whether one wants to obtain the basis images or their mixing coefficients to be independent. These two approaches are called, respectively, ICA₁ and ICA₂ architectures [1].

1) *ICA₁ Architecture*: In this architecture, each of N individual hand-data is assumed to be a linear mixture of an unknown set of N statistically independent source hands. For this

$$\begin{aligned}
 \mathbf{x}_i &= A(i,1) \times \hat{\mathbf{s}}_1 + A(i,2) \times \hat{\mathbf{s}}_2 + \dots + A(i,N) \times \hat{\mathbf{s}}_N \\
 \text{ICA}_1 \text{ representation for } i^{\text{th}} \text{ hand: } \mathbf{a}_i &= [A(i,1), A(i,2), \dots, A(i,N)] \\
 \mathbf{x}_i &= \mathbf{a}_1 \times \hat{P}(1,i) + \mathbf{a}_2 \times \hat{P}(2,i) + \dots + \mathbf{a}_N \times \hat{P}(N,i) \\
 \text{ICA}_2 \text{ representation for } i^{\text{th}} \text{ hand: } \hat{\mathbf{p}}_i &= [\hat{P}(1,i), \hat{P}(2,i), \dots, \hat{P}(N,i)]
 \end{aligned}
 \tag{a}$$

$$\tag{b}$$

Fig. 7. Decomposition of hand images into ICA patterns: (a) patterns in ICA₁ architecture and (b) patterns in ICA₂ architecture.

model, images of normalized hands, of size 200×200 , are raster scanned to yield data vectors of size 40 000. Note that the data matrix \mathbf{X} will be $N \times 40\,000$ dimensional. This matrix is decomposed into N independent source components $\{\hat{\mathbf{s}}_i\}$, which will take place along the rows of the output matrix $\hat{\mathbf{S}}$. Each row of the mixing matrix \mathbf{A} ($N \times N$) will contain weighting coefficients specific to a given hand. These weights show the relative contribution of the source hands to synthesize a given sample hand [Fig. 7(a)]. It follows then that, for the hand \mathbf{x}_i , the i^{th} row of \mathbf{A} will constitute an N -dimensional feature vector. In our work, N was equal to the number of subjects, that is, of “hand sources.” In the recognition stage, assuming that the test set follows the same synthesis model with the same independent components, we project a normalized test hand \mathbf{x}_{test} ($1 \times 40\,000$), onto the set of predetermined basis functions and compare the resulting vector of projection coefficients given by

$$\mathbf{a}_{\text{test}} = \mathbf{x}_{\text{test}} \hat{\mathbf{S}}^T (\hat{\mathbf{S}} \hat{\mathbf{S}}^T)^{-1}. \tag{14}$$

Finally, the individual to be tested is recognized as the individual i^* when \mathbf{a}_{test} is closest to the feature vector \mathbf{a}_{i^*} and where the distance is measured with L1 metric

$$i^* = \arg \min_i \left\{ \sum_{j=1}^N |a_{i,j} - a_{\text{test},j}| \right\}. \tag{15}$$

2) *ICA₂ Architecture:* In this second architecture, the superposition coefficients are assumed to be independent, but not the basis images. Thus, this model assumes that, each of K pixels of the hand images result from independent mixtures of random variables, that is the “pixel sources.” For this purpose, we start considering the transpose of the data matrix: \mathbf{X}^T . However, the huge dimensionality of pixel vectors (typically $K \gg N$) necessitates a PCA reduction stage prior to ICA.

In fact, the eigenvectors of the $K \times K$ covariance matrix

$$\mathbf{C} = \frac{1}{N} \mathbf{X}^T \mathbf{X} \tag{16}$$

where each row of \mathbf{X}^T is centered, can be calculated by using the eigenvectors of the much smaller $N \times N$ matrix $\mathbf{X} \mathbf{X}^T$.

Let $\{\mathbf{v}_1, \dots, \mathbf{v}_M\}$ be the M ranked eigenvectors with eigenvalues $\{\lambda_1 \geq \lambda_2 \geq \dots \geq \lambda_M\}$ of the $N \times N$ matrix $\mathbf{X} \mathbf{X}^T$. Then, by SVD theorem [10], the orthonormal eigenvectors $\{\boldsymbol{\omega}_1, \dots, \boldsymbol{\omega}_M\}$ of \mathbf{C} corresponding to the $M \leq N$ largest eigenvalues $\{\lambda_1, \dots, \lambda_M\}$ are

$$\boldsymbol{\omega}_j = \frac{1}{\sqrt{\lambda_j}} \mathbf{X}^T \mathbf{v}_j \tag{17}$$

where $j = 1, \dots, M$. After the projection of input vector \mathbf{x} onto the j^{th} eigenvector $\boldsymbol{\omega}_j$, we obtain the j^{th} feature as

$$y_j = \frac{1}{\sqrt{\lambda_j}} \mathbf{v}_j^T \mathbf{X} \mathbf{x}^T. \tag{18}$$

Thus, the feature vector is given by

$$\mathbf{y} = \mathbf{R} \mathbf{x}^T \tag{19}$$

where \mathbf{R} represents the $M \times K$ projection operator formed by $\boldsymbol{\omega}_j$'s in its rows. The hand image data is reduced after being projected on the few $M = N$ principal components and thus forms the $(N \times N)$ square data matrix $\mathbf{R} \mathbf{X}^T$. Finally we decompose $\mathbf{R} \mathbf{X}^T$ to source and mixing coefficients according to the model in Fig. 7(b), we obtain our basis functions (the hand images) in the columns of the estimated mixing matrix $\hat{\mathbf{A}}$, which is $N \times N$. Conversely, the coefficients in the estimated source matrix are statistically independent. The synthesis of a hand in the data set \mathbf{x}_i , from superposition of hand “basis images” as in the columns of $\hat{\mathbf{A}}$, is illustrated in Fig. 7(b).

In the recognition stage, assuming again that test hands follow the same model, they are also size reduced with $\mathbf{R} \mathbf{x}_{\text{test}}^T$, and multiplied by the de-mixing matrix

$$\mathbf{W} = \mathbf{A}^{-1}. \tag{20}$$

The resulting coefficient vector of a test hand \mathbf{x}_{test} ($1 \times K$), found as

$$\hat{\mathbf{p}}_{\text{test}} = \mathbf{W} \mathbf{R} \mathbf{x}_{\text{test}}^T \tag{21}$$

which is then compared with predetermined feature vectors of the training stage. Notice that we use a different symbol ($\hat{\mathbf{p}}$) for

the demixing outputs in the ICA_2 model denoting “hand pixel sources” as compared to the ICA_1 model, where (\hat{s}) was used to denote “hand shape sources.” Finally, the individual to be tested is simply recognized as the person i^* with the closest feature vector $\hat{\mathbf{p}}_{i^*}$, where distance is measured in terms of cosine of the angle between them

$$i^* = \arg \max_i \left\{ \frac{\hat{\mathbf{p}}_i \bullet \hat{\mathbf{p}}_{\text{test}}}{\|\hat{\mathbf{p}}_i\| \|\hat{\mathbf{p}}_{\text{test}}\|} \right\}. \quad (22)$$

Let us recall again the parameters: the number of pixels in the hand images was $K = 40\,000$, and the dimension of the subspace, M , was taken equal to the number of individuals, that is, $M = N$.

IV. EXPERIMENTAL RESULTS

A. Data Acquisition

Our hand database contained 1374 images of hands of 458 different persons, as we collected from each person three images both of the right hands [9]. The images were acquired with a HP Scanjet 5300 c scanner at 45-dpi resolution; hence, the images measured 383×526 pixels in the preprocessing stage. The segmentation, pose normalization and ring removal algorithms were run on this resolution images. The images were further reduced to 20-dpi resolution (and cropped to 200×200 pixels) at the feature extraction stage, that is, when the ICA parameters were extracted. There were no control pegs to orient the fingers, and there were no restrictions on hand accessories, like rings. In our case, the imaging conditions that yielded the desired images were the pressure, albeit slight, that the subjects exerted on the platen, plus the awareness of keeping fingers apart. Notice that all other schemes in the literature demand that the fingers be kept apart. None of the hands and/or images had to be discarded. The subjects were Turkish and French students and staff members from various levels, departments and universities in the age span of 20–50. They were not habituated to the system beforehand, and they were told simply to keep their fingers apart and their hands off from the boundaries. In a real-life situation, we believe a user would be even more cooperating if the subject were confronted with actual denial of access. Each person underwent three hand scan sessions within intervals of five to ten minutes, and between the sessions the subject could add or remove, at will, rings, or roll up or down sleeves. We also acquired hand images after about six months from a subset of the subjects that we could track, in order to assess the accuracy of the system after a long time interval.

First, the hand recognition experiments, based on normalized hand images, were performed on five selected population sizes, namely, population subsets consisting of 20, 35, 50, 100, and 458 individuals. The rationale of the choice of these subpopulations was that they were the enrollment sizes used in the literature. Different population sizes help us perceive the recognition performance with increasing number of individuals. A boosting algorithm was applied so that several different formations of subsets (of sizes of 20, 35, 50, and 100) were created by random choice and their performance scores were averaged.

TABLE III
CORRECT IDENTIFICATION PERFORMANCE AS A FUNCTION
ENROLLMENT SIZE (DOUBLE TRAINING SET)

Method	Correct identification percentage				
Hand set size	20	35	50	100	458
Hausdorff	98.75	98.14	97.97	97.21	93.51
ICA_1	98.25	97.91	97.67	97.00	93.45
ICA_2	99.48	99.40	99.27	98.81	97.31

B. Identification Results

The modified Hausdorff distance-based recognition yields the results shown in Table III, where the numbers of contour elements were made equal to $N_f = N_g = 2048$ via interpolation and resampling. We have noticed that most of the errors occur due to the guillotined artifact of the wrist. We tried different weights to counter the effect of the wrist ambiguity [18], and it turned out that discounting the wrist area completely resulted in the best performance. The Hausdorff results are shown in the bar charts in Fig. 8 with one variance-long whisker. The correct recognition results using ICA features are given also in Table III. These feature vectors correspond, respectively, to mixture coefficients of independent hand shape sources and to source pixels of hand images. In the ICA_2 architecture we used not necessarily N -dimensional features but the feature dimension yielding the best score. For example, for the enrollment size of 458 the feature dimensionality was 200, and not 458. We have noticed that the second ICA architecture (ICA_2) performed better than the first architectures, namely, ICA_1 . The satisfactory results indicate that the independent component analysis features, whether in the form of mixture coefficients or in the form of source hands, capture in a small subspace, the information necessary for person discrimination.

Second, we wanted to see the effect of training sample size, that is, the impact of multiple independent recordings of the individual’s hand. Thus, we ran the recognition experiments with a single training and then with the double training set, both in a round robin fashion. More explicitly, let the three sets of hand images subjects be referred to as the sets A, B, C. In the single set experiments, the ordering of the test and training sets were $\{(A,B), (B,A), (A,C), (C,A), (B,C), (C,B)\}$. In other words, set A hands were tested against the training set of set B etc. In the double training set, the ordering of the test and training sets were $\{(A, BC), (B, AC), (C, AB)\}$, e.g., hands in the test set A were recognized using hands both in the sets B and C. Finally, the recognition scores were averaged from these training and test set combinations. Table IV indicates that there is significant improvement when one shifts from single-training set to the double training set. One can notice that the increase in the size of the training set has a nonnegligible effect on the identification performance. The effect becomes more pronounced for increasing enrollment sizes and the contribution is higher in the case of the Hausdorff-based technique.

C. Verification Results

We ran verification experiments where the “genuine hands” had to be differentiated from the “impostor hands.” We calcu-

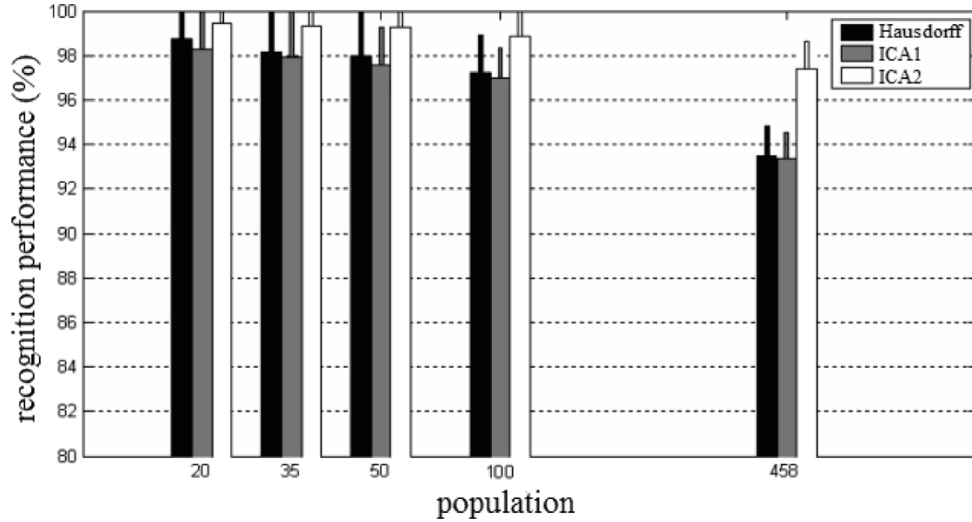


Fig. 8. Bar charts of average recognition accuracy as a function of test size for the ICA₁, ICA₂ and Hausdorff schemes. The whiskers have the size of one variance (double training set).

TABLE IV
EFFECT OF TRAINING SET SIZE ON THE IDENTIFICATION PERFORMANCE:
THE PERCENT POINT IMPROVEMENT SHOWN BETWEEN
THE SINGLE- AND DOUBLE-TRAINING SET

Hand set size	20	35	50	100	458
Hausdorff	2.67	3.23	4.23	4.38	3.61
ICA ₁	0.75	1.07	1.27	2.17	3.39
ICA ₂	0.54	1.31	1.33	2.23	2.36

late the distances between the hand shape of the applicant and the hand shapes collected in the database of the subject that he claims to be, and then comparing this score against a threshold. If this distance is below the threshold than the claimant is accepted as true; otherwise he is rejected. In the case an impostor presents himself and his distance to the claimed hands is below the threshold, then we have a false acceptance. Conversely, if the distance between the applicant's hand and those registered in the database is above the threshold we have a case of false rejection. In Figs. 9 and 10, we plot the distance histograms for the two approaches, namely the histogram of Hausdorff distances as in (10) and (11), and the histogram of the Euclidean distances of the ICA₂ feature, as in Section IV-B, that is, $\|\hat{\mathbf{p}}_i - \hat{\mathbf{p}}_{\text{test}}\|^2$, $i \in \text{database}$. In both figures, the left histogram describes the distribution of intra distances (genuine hands), while the right histogram is the distribution of inter differences (impostor hands). The receiver operating characteristic (ROC) curves are plotted in Figs. 9(b) and 10(b). The verification comparisons between the three feature modalities are given in Table V as a function of enrollment size. Notice that for smaller populations (sizes 20, 35, 50 and 100, 458), the performance is calculated as the average of several randomly chosen subject sets. If C snapshots are stored in the database from each of the N enrolled individuals, then the genuine distance histograms are calculated by $N \times C!/[2(C-2)!]$ genuine (intra) measurements, and the impostor (inter) distance histograms by $C^2 \times N \times (N-1)/2$ measurements. For example, in our case the enrollment size is $N = 458$ and the number of snapshots is $C = 3$; hence, the number of distance pairs computed to obtain genuine distance

histograms is 1374, and the number is 941 877 for the impostor distance histograms.

D. Comparison of Identification and Verification Performances With Existing Algorithms

We have compared the performance of our algorithm with that of the other algorithms in the literature. These scores were gleaned from the papers in the literature or read off from their ROC curves. In Table VI, we compare the identification performances, while, in Table VII, verification performance figures are provided. While these comparisons gives an idea about the state of the art, one caveat is that the images are acquired with different techniques, namely with digital scanner and digital camera, albeit at approximately the same resolution. Also notice that we have adapted our population sizes to those available in the literature, but some methods were excluded, e.g., [19], since their ROC curves were not available.

One can observe that in both identification and verification tasks, our scheme based on ICA₂ architecture outperforms all of its competitors in the literature, except for [17], which uses in addition to shape features, texture features as well.

E. Accuracy of Hand Biometry Over Time

In realistic environments, enrolled subjects can present themselves at arbitrary intervals. We wanted to test if the hand-biometry system can maintain its accuracy over larger lapses of time. From a subset of 74 subjects that we could track, we recorded hand images after an average interval of six months, time lapses actually varying between 20 and 30 weeks. Fig. 11(a) shows the box-and-whisker plots of ICA₂ feature distances, while Fig. 11(b) illustrates the identification performance. One can see that the intra-distances between hands recorded within an interval of six months almost overlaps with those recorded within the same day. For this subset, there was no performance difference in identification or verification. However, as the time-elapsd subset is augmented, one can expect some performance deterioration as hinted by the slight shift of the intra-distance statistics toward the interdistance histogram.

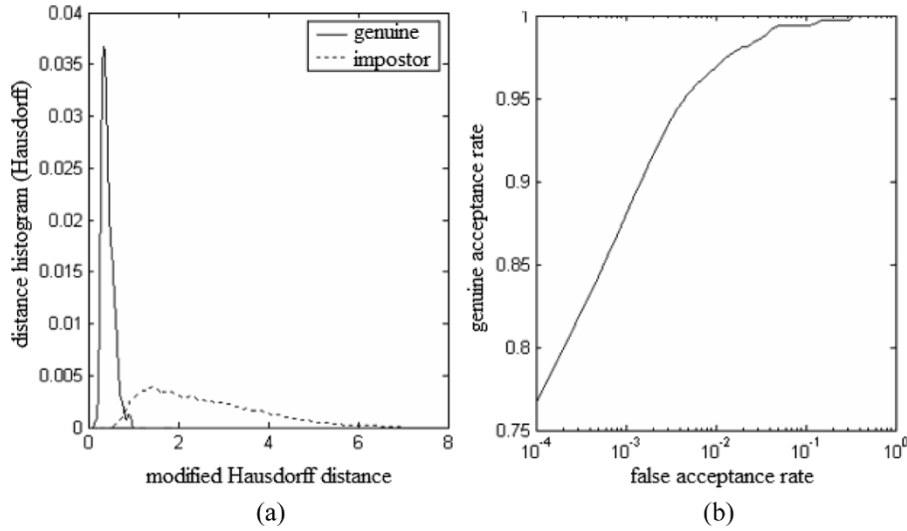
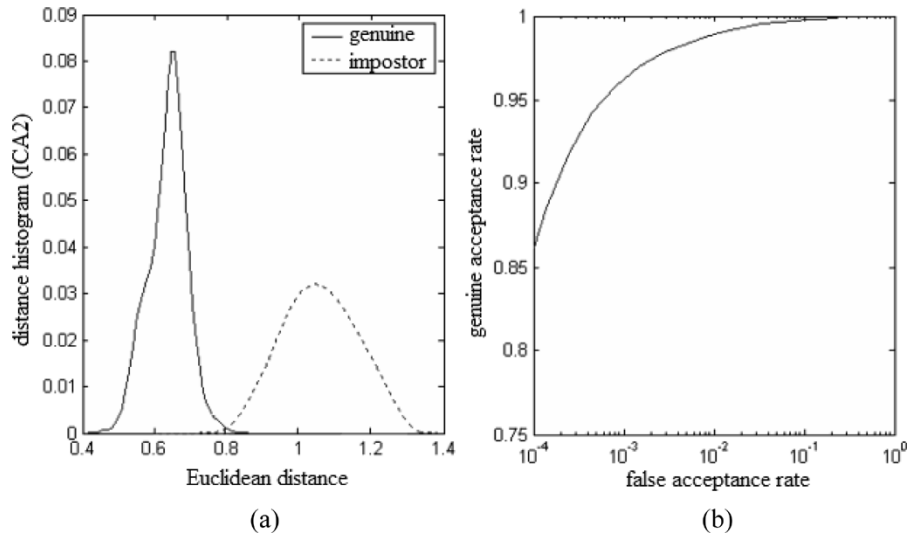


Fig. 9. Verification results of the Hausdorff-distance based method: (a) genuine and impostor distributions and (b) ROC curve.

Fig. 10. Verification results of the ICA₂-based method: (a) genuine and impostor distance histograms and (b) ROC curve.TABLE V
VERIFICATION PERFORMANCE AS A FUNCTION
OF ENROLLMENT SIZE (EQUAL ERROR RATE)

Method	Verification percentage				
Hand set size	20	35	50	100	458
Hausdorff	99.16	98.87	98.72	98.04	97.36
ICA ₁	99.05	98.81	98.83	98.03	97.23
ICA ₂	99.55	99.48	99.40	98.85	98.21

TABLE VI
COMPARISON OF RECOGNITION PERFORMANCE OF ALGORITHMS
FOR GIVEN ENROLLMENT SIZES (AVAILABLE RESULTS)

Enrollment size	Best performance in the literature	Our performance (ICA ₂)
20	97.0 [22]	99.48
35	95.0 [19]	99.40
70	98.5 [2,28]	99.03
458	-	97.31

TABLE VII
COMPARISON OF THE VERIFICATION PERFORMANCE OF ALGORITHMS FOR
DIFFERENT POPULATION SIZES (THE FIGURES QUOTED ARE AT THE
EQUAL FALSE ALARM-FALSE REJECT POINT)

Enrollment size	Best performance in the literature	Our performance (ICA ₂)
20	94.5 [22]	99.55
50	97.5 [8]	99.40
100	99.1 [17]	98.85
458	-	98.21

V. CONCLUSION

We have shown that hand shape can be a viable scheme for recognizing people with high accuracy, at least for population of sizes within hundreds. In that respect we believe the scorecard of the hand geometry modality can be promoted to “high” in the distinctiveness and performance attributes, in the comparison in [14]. Furthermore, the biometric modality based on the hand geometry constitutes an unobtrusive method

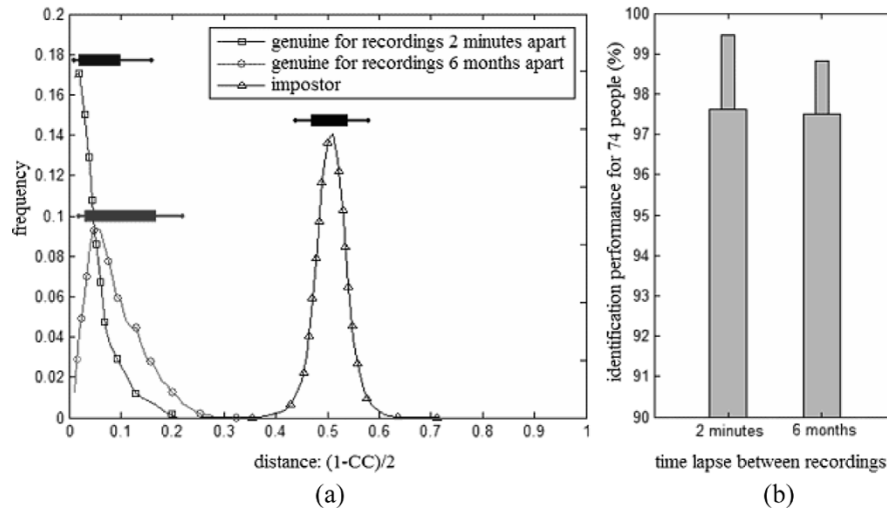


Fig. 11. (a) Genuine and impostor distributions with various time lapses and (b) ICA_2 mean identification performances for a population of 74 people with various time lapses.

of person recognition in that the interface is user-friendly and it is not subject to variability to the extent faces are under confounding factors of accessories, illumination effects and expression. Preliminary tests indicate that hand biometric accuracy is maintained over span of time. For any hand-based recognition scheme, it is imperative, however, that the hand image be preprocessed for normalization so that hand attitude in general, and fingers in particular be aligned to standard positions. Presently a straightforward Matlab code requires 5–6 s to process hands; which implies that with an optimized C code, the recognition and/or verification system can run at real time, that is, under 1 s.

Several other paths of research remain to be explored. For example, other feature extraction schemes such as axial radial transform (ART) [15], Fisher hands or kernelized versions of principal component analysis or linear discriminant analysis can be tried. Normalization of hands based on active contours [5], provided reliable landmarks can be initially obtained, is another alternative. Fusion schemes at the data, feature and decision level with multiple snapshots, multiple units (right and left hands) and multiple matchers (e.g., ICA and ART) can be envisioned. The hand color and texture and/or the palm print [11], [26], in addition to the hand shape could be judiciously combined to enhance recognition. We believe the ICA representation will be a method to capture both hand-shape information and palmprint patterns in one scheme.

In this study, only the right hands of people have taken a role. The improvement in the recognition rate with the use of the images of both hands or with a more extended set of training images, i.e., more than two images per person must be studied. More challenging imaging scenarios can be considered that obviate physical contact between the hand and the imaging device, but in turn introducing additional variability in lighting, hand orientation and distance. Finally, building the system and testing under real-life conditions can prove more rigorously the viability of hand-based access scheme, including the execution time for preprocessing and comparisons.

REFERENCES

- [1] M. S. Bartlett, H. M. Lades, and T. J. Sejnowski, "Independent component representations for face recognition," presented at the Conf. Human Vision and Electronic Imaging III, San Jose, CA, 1998.
- [2] Y. Bulatov, S. Jambawalikar, P. Kumar, and S. Sethia, "Hand recognition using geometric classifiers," presented at the ICBA Int. Conf. Bioinformatics and its Applications, FL, Dec. 16–19, 2004.
- [3] [Online]. Available: <http://www.gwc.maricopa.edu/class/bio201/hand/anhand.htm>
- [4] J. F. Canny, "A computational approach to edge detection," *IEEE Trans. Pattern Anal. Mach. Intell.*, vol. PAMI-8, no. 6, pp. 679–698, Jun. 1986.
- [5] T. F. Cootes, G. J. Edwards, and C. J. Taylor, "Active appearance models," *IEEE Trans. Pattern Anal. Mach. Intell.*, vol. 23, no. 6, pp. 681–685, Jun. 2001.
- [6] B. A. Draper, K. Baek, M. S. Bartlett, and J. R. Beveridge, "Recognizing faces with PCA and ICA," *Comput. Vis. Image Understand.*, vol. 91, no. 1–2, pp. 115–137, 2003.
- [7] M. P. Dubuisson and A. K. Jain, "A modified Hausdorff distance for object matching," presented at the 12th Int. Conf. Pattern Recognition, Jerusalem, Israel, 1994, pp. 566–568.
- [8] A. K. Jain and N. Duta, "Deformable matching of hand shapes for verification," presented at the Int. Conf. Image Processing, Oct. 1999.
- [9] S. Garcia-Salicetti, C. Beumier, G. Chollet, B. Dorizzi, J. L. les Jardins, J. Lunter, Y. Ni, and D. Petrovska-Delacretaz, "Biomet: A multimodal person authentication database including face, voice, fingerprint, hand and signature modalities," presented at the Int. Conf. Audio- and Video-based Biometric Person Authentication, Guildford, U.K., Jun. 9–11, 2003.
- [10] G. H. Golub and C. F. van Loan, *Matrix Computation*, 3rd ed. Baltimore, MD: Johns Hopkins Univ. Press, 1996.
- [11] C. C. Han, H. L. Cheng, C. L. Lin, and K. C. Fan, "Personal authentication using palm print features," *Pattern Recognit.*, vol. 36, pp. 371–381, 2003.
- [12] J. Himberg and A. Hyvärinen, "Independent component analysis for binary data: An experimental study," presented at the Int. Workshop Independent Component Analysis and Blind Signal Separation, San Diego, CA, 2001.
- [13] A. Hyvärinen and E. Oja, "Independent component analysis: algorithms and applications," *Neural Netw.*, vol. 13, no. 4–5, pp. 411–430, 2000.
- [14] A. K. Jain, A. Ross, and S. Prabhakar, "An introduction to biometric recognition," *IEEE Trans. Circuits Syst. Video Technol.*, vol. 14, no. 1, pp. 4–20, Feb. 2004.
- [15] S. Jeannin, "MPEG-7 visual part of eXperimentation model, version 9.0," presented at the ISO/IEC JTC1/SC29/WG11/N3914, 55th, Mpeg Meeting, Pisa, Italy, Jan. 2001.
- [16] B. B. Kimia, I. Frankel, and A. M. Popescu, "Euler spiral for shape completion," *Int. J. Comput. Vis.*, vol. 54, no. 1/2, pp. 157–180, 2003.
- [17] Y. A. Kumar, D. C. M. Wong, H. C. Shen, and A. K. Jain, "Personal verification using palmprint and hand geometry biometric," in *Proc. 4th Int. Conf. Audio Video-Based Biometric Person Authentication*, Guildford, U.K., Jun. 9–11, 2003, pp. 668–678.

- [18] K. H. Lin, K. M. Lam, and W. C. Siu, "Spatially eigenweighted Hausdorff distances for human face recognition," *Pattern Recognit.*, vol. 36, pp. 1827–1834, 2003.
- [19] C. Öden, A. Erçil, and B. Büke, "Combining implicit polynomials and geometric features for hand recognition," *Pattern Recognit. Lett.*, vol. 24, pp. 2145–2152, 2003.
- [20] A. K. Jain, A. Ross, and S. Prabhakar, "Biometrics-Based Web Access," MSU Tech. Rep. TR98-33, 1998.
- [21] A. K. Jain, A. Ross, and S. Pankanti, "A prototype hand geometry based verification system," in *Proc. 2nd Int. Conf. Audio- and Video-Based Biometric Person Authentication*, Mar. 1999, pp. 166–171.
- [22] R. Sanchez-Reillo, C. Sanchez-Avila, and A. Gonzalez-Marcos, "Biometric identification through hand geometry measurements," *IEEE Trans. Pattern Anal. Mach. Intell.*, vol. 22, no. 10, pp. 1168–1171, Oct. 2000.
- [23] B. Takacs, "Comparing face images using the modified Hausdorff distance," *Pattern Recognit.*, vol. 31, no. 12, pp. 1873–1881, 1998.
- [24] A. R. Weeks, *Fundamentals of Electronic Image Processing*. New York: SPIE, 1996, pp. 466–467.
- [25] C. Xu and J. L. Prince, "Snakes, shapes, and gradient vector flow," *IEEE Trans. Image Process.*, vol. 7, no. 3, pp. 359–369, Mar. 1998.
- [26] D. Zhang, W. K. Kong, J. You, and M. Wong, "Biometrics-online palmprint identification," *IEEE Trans. Pattern Anal. Mach. Intell.*, vol. 25, no. 9, pp. 1041–1050, Sep. 2003.
- [27] R. L. Zunkel, "Hand geometry based verification," in *Biometrics*, A. Jain, R. Bolle, and S. Pankanti, Eds. Norwell, MA: Kluwer, 1999, pp. 87–101.
- [28] P. Kumar, "Clustering and reconstructing large data sets," Ph.D. dissertation, Stony Brook Univ., Stony Brook, NY, 2004.



Erdem Yörük was born in Ankara, Turkey, in 1978. He received the B.Sc. and M.Sc. degrees from the Department of Electrical and Electronic Engineering, Bogaziçi University, Istanbul, Turkey, in 2002 and 2004, respectively, where he is currently pursuing the Ph.D. degree.

He is currently a Research Assistant in the Bogazici University Signal and Image Processing Laboratory. His major field of study is telecommunications and signal processing. His research interests include computer vision, pattern recognition,

biometrics, medical image analysis, computational anatomy, and applied mathematics.

Mr. Yörük shared the Best Student Paper Award with Ender Konukoğlu at the IEEE-SIU 2004 Conference for the paper entitled "Shape based hand recognition."



Ender Konukoğlu was born in Istanbul, Turkey, in 1981. He received the B.Sc. and M.Sc. degrees from the Department of Electrical and Electronic Engineering, Bogaziçi University, Istanbul, Turkey, in 2003 and 2005, respectively.

Currently, he is a Research Assistant with the Bogazici University Signal and Image Processing Laboratory. His major field of study is telecommunications and signal processing. His research interests include medical image analysis, biometrics, and partial differential equations in image processing.

Mr. Konukoğlu shared the Best Student Paper Award with Erdem Yörük at the IEEE-SIU 2004 Conference for the paper entitled "Shape based hand recognition."



Bülent Sankur (S'70–M'76–SM'90) received the B.Sc. degree from Bogaziçi University, Istanbul, Turkey, and the M.Sc. and Ph.D. degrees from Rensselaer Polytechnic Institute, Troy, NY.

He has been active in the Department of Electric and Electronic Engineering, Bogaziçi University, establishing curricula and laboratories and guiding research in the areas of digital signal processing, image and video compression, biometry, and multimedia systems. He has held visiting positions at the University of Ottawa, Ottawa, ON, Canada; Istanbul

Technical University; the Technical University of Delft, Delft, The Netherlands; and the Ecole Nationale Supérieure des Telecommunications, Paris, France.

Dr. Sankur was the Chairman of the 1996 International Telecommunications Conference, the 2005 European Signal Processing Conference, and the Technical Co-Chairman of ICASSP 2000.



Jérôme Darbon was born in Chenôve, France, in 1978. He received the M.Sc. degree in applied mathematics from the E.N.S. de Cachan, Cachan, France. He is currently pursuing the Ph.D. degree at the Ecole Nationale Supérieure des Télécommunications, Paris, France.

His main research interests include fast algorithms for exact energy minimization and mathematical morphology.